Co-published by
Institute of Fluid-Flow Machinery
Polish Academy of Sciences
Committee on Thermodynamics and Combustion
Polish Academy of Sciences

Copyright©2025 by the Authors under licence CC BY-NC-ND 4.0

http://www.imp.gda.pl/archives-of-thermodynamics/

A theoretical investigation of magnetohydrodynamics, couple stress and viscosity variation on squeeze film lubrication between a cylinder and rough porous flat surface

Suresha Ramareddy[a*], Arunkumar Rudrappa[b], Bannihalli Naganagowda Hanumagowda[c], Subramanya Raghavendra[d]

[a]Department of Mathematics, Jain (Deemed-to-be University), Kanakapura Taluk, Ramanagara District 562112, Karnataka, India
[b]Department of Mathematics, Sai Vidya Institute of Technology, Bangalore 560064, Karnataka, India
[c]Department of Mathematics, GM University, Davangere 577006, Karnataka, India
[d]Department of Mechanical Engineering, Sai Vidya Institute of Technology, Bangalore 560064, Karnataka, India
*Corresponding author email: suresharamareddy@gmail.com

Received: 14.03.2025; revised: 16.09.2025; accepted: 29.10.2025

Abstract

Squeeze film lubrication involving couple stress fluids, viscosity variation and magnetohydrodynamics is critically important for high-performance applications in automotive systems, aerospace mechanisms and biomedical devices. This study aims to examine the combined influence of these effects on lubrication performance between a cylinder and a rough porous flat surface. To achieve this, we developed a generalised modified Reynolds equation by integrating Christensen's stochastic model for surface roughness, Darcy's law for porous media flow, and Stokes flow theory. This equation was solved with appropriate boundary conditions to derive analytical expressions for pressure, enabling the calculation of load-carrying capacity and squeeze film time for both longitudinal and transverse roughness patterns. Key findings demonstrate that couple stress, magnetohydrodynamics effects, and viscosity variation significantly enhance pressure distribution, increasing load-carrying capacity by up to 85.29% and squeeze film time by up to 85.34% under optimal conditions. Notably, longitudinal roughness pattern degrades tribological performance, whereas transverse roughness pattern enhances it. Furthermore, three-dimensional analysis demonstrates that optimal tuning of roughness and porosity parameters maximises the system performance. These findings, validated against established results like Lin et al. [31], provide valuable design guidelines for optimising tribological systems in fields requiring precise and durable lubrication, particularly in precision manufacturing and microelectromechanical systems.

Keywords: Magnetohydrodynamics; Porous, Rough surface; Viscosity variation

Vol. 46(2025), No. 4, 141–156; doi: 10.24425/ather.2025.156845

Cite this manuscript as: Ramareddy, S., Rudrappa, A., Hanumagowda, B.N., & Raghavendra, S. (2025). A theoretical investigation of magnetohydrodynamics, couple stress, and viscosity variation on squeeze film lubrication between a cylinder and rough porous flat surface. *Archives of Thermodynamics*, 46(4), 141−156.

1. Introduction

Surface roughness in combination with a porous medium influenced by magnetohydrodynamics (MHD) holds significant practical applications, particularly in industries such as aircraft design. However, the presence of surface roughness is crucial for understanding how components interact with their surroundings. Nevertheless, excessive surface roughness may not yield beneficial outcomes. Surface roughness serves as an appropriate indicator of physical component efficiency, as irregularities on surfaces can lead to areas of nucleation for cracking, rusting or breakdown, and rough surfaces tend to exhibit higher coefficients of friction compared to smoother surfaces. In practical scenarios, all bearing surfaces inherently exhibit some degree of

Nomenclature

B_0 – magnetic field applied externally, Wb/m^2
c – roughness factor
C – dimensionless roughness
D – cylinder's length, mm
$g(h_s)$– probability density function
G – viscosity parameter
h – thickness of the film, mm
h_m – minimal film thickness, mm
h_{m0} – initial minimal thickness of the film, mm
h_S – stochastic film thickness, mm
k – porous medium factor
l^* – dimensionless couple stress, $l^* = 2l/h_{m0}$
m – magnetic moment of the particle, A m^2
M_0 – Hartmann number
p^* – pressure in the porous area, Pa
P – pressure, Pa
P^* – dimensionless pressure
R – cylinder's radius, mm
R_{T^*} – relative frequency of squeeze film time
R_{W^*}– relative frequency of load-carrying capability
T^* – dimensionless squeeze film time
u, w– velocity factor in the x and z direction, mm/s
u^*, w^*– Darcy's velocity factor in the permeable area, mm/s
V – velocity of squeezing, mm/s
W^* – dimensionless load-carrying capability

Greek symbols

α – viscosity coefficient
β – microstructure to the size of pore ratio, $\beta=(\eta/\mu)/k$
δ – porous layer thickness, mm
η – material constant, N s
μ – dynamic viscosity, cP
μ_0 – initial velocity, mm/s
σ – lubricant electrical conductivity, S/m
$\bar{\sigma}$ – standard deviation
ψ – porous factor

Abbreviations and Acronyms

MEMS – Microelectromechanical systems
MHD – Magnetohydrodynamics

roughness, including porous bearings, which are typically designed for low-load operations. Surface roughness significantly affects lubrication, influencing critical performance parameters such as load-bearing capability, pressure and response time. Recent studies have explored various factors influencing squeeze film lubrication under various circumstances. Bujurke et al. [1] explored the impacts of roughness on squeeze film lubrication among curved-shaped annular surfaces, deriving a modified Reynolds equation using Christensen's stochastic method. Their findings revealed that circumferential roughness increases the load-bearing capability while shifting the pressure maximum towards the outlet edge, whereas radial roughness decreases the load capacity. Christensen [2], through a stochastic theory approach, demonstrated that surface roughness considerably impacts bearing characteristics, with its effect dependent on roughness type but not critically on the distribution function. Daliri and Jalali-Vahid [3] extended this by incorporating viscosity-pressure dependency and non-Newtonian fluid effects, showing an improved squeeze film performance for circular surface roughness patterns, while radial patterns led to a reduction in squeeze film performance. Further, Mouda et al. [4] examined MHD non-parallel lubrication with non-Newtonian fluids and identified significant interactions among MHD, surface roughness and non-Newtonian effects. Dass et al. [5] highlighted that velocity-slip and ferrofluid lubrication, combined with couple stress and surface roughness, greatly enhance pressure and load-carrying capacity under magnetic fields. Other studies, such as Ullah et al. [6] and Johny et al. [7], explored MHD flows in porous media, emphasising how magnetic fields and porosity influence velocity profiles and load capacity, respectively. Yadav and Srivastava [8] explored immiscible fluid dynamics in porous channels, validating the use of porous materials for flow control. Patel et al. [9] examined ferrofluid lubrication in porous squeeze films, finding significant performance enhancements using specific magnetic fluid flow models. Similarly, Khan et al. [10] and Patel and Deheri [11] demonstrated improvements in squeeze film characteristics due to magnetic effects, couple stress fluids, and surface roughness. Lin et al. [12] developed a two-dimensional Reynolds expression for non-Newtonian fluids, showing increased load capacity with couple stresses and magnetic fields. Nabhani and El Khlifi [13] further confirmed the benefits of magnetic fields, couple stress and fluid inertia on squeeze film performance. Ramasamy [14] emphasised the effect of non-Newtonian thixotropic fluids on squeeze film behaviour, with higher load capacity attributed to increased yield numbers and Hartmann parameters. Jyothi et al. [15] extended this to sphere-flat plate systems, demonstrating the detrimental effects of slip velocity despite enhancements from couple stress.

Squeeze film lubrication has advanced by integrating factors like surface roughness and porous materials, enhancing our understanding of lubrication dynamics. For instance, Prakash et al. [16] utilised stochastic theory to examine the hydrodynamic lubrication effects on rough surfaces between rotating annular discs, highlighting the interplay between porous facings and film pressure. Shah [17] extended these investigations to ferrofluid-lubricated circular disc designs under variable magnetic fields, demonstrating how circumferential roughness and radial permeability affect load-carrying capacity in different bearing configurations. Thakkar and Patel [18] provided a comprehensive analysis of the MHD-based squeeze film among porous circular surfaces, concluding that magnetisation significantly enhances load capacity, while negatively skewed roughness contributes positively to bearing efficiency. Vadher et al. [19] expanded the scope to conducting rough, porous elliptical plates, illustrating that hydromagnetic lubrication offsets the adverse effects of transverse surface roughness and porosity through the synergistic impact of conductivity and magnetisation. Deheri and Patel [20] applied a stochastic framework to study magnetic fluid-lubricated rough, porous parallel plates, revealing that porosity decreases load-carrying capacity but can be mitigated by

proper roughness and magnetic parameters. Anthony and Elamparithi [21] analysed a couple stress fluids in rough-porous Rayleigh step slide bearings under MHD, noting that roughness increased both workload and frictional forces. Ali et al. [22] investigated non-Newtonian fluids across oscillatory extending sheets in porous media, finding viscosity variations and couple stresses to amplify velocity oscillations and skin friction. Studies by Naduvinamani and Siddangouda [23] emphasised the influence of azimuthal and radial roughness patterns on squeeze film lubrication among porous circular-shaped stepped surfaces, while Vashi et al. [24] demonstrated how ferrofluid and negatively skewed roughness parameters enhance bearing performance for longitudinally rough stepped plates.

Significant progress has been made in squeeze film lubrication research, with numerous studies examining the impacts of roughness, porosity, couple stress, viscosity variation and MHD on lubrication attributes. Prakash and Gururajan [25] examined the influence of slip velocity on rough, porous journal bearings. Applying Christensen's stochastic theory for rough surfaces at the porous region, they derived modified Reynolds expressions for different roughness patterns and demonstrated that roughness-slip relations significantly alter bearing efficiency. Rahul and Rao [26] investigated the flow behaviour of Rabinowitsch fluids in a porous medium, incorporating viscosity variation and surface roughness effects on circular stepped plates. Their theoretical findings revealed that surface roughness and porosity decrease (increase) load-bearing capability and squeeze film time for radial (azimuthal) roughness, whereas viscosity enhances load-bearing capability and reduces squeeze film time in comparison with smooth, isoviscous surfaces. Sangeetha and Kesavan [27] extended these analyses to a couple stress MHD squeeze films in rough, porous rectangular-shaped surfaces, concluding that the magnetic field significantly enhances pressure compared to the Newtonian case. Similarly, Masood and Elamparithi [28] studied finite plates lubricated with non-Newtonian fluids under a transverse MHD and noted that viscosity variation and roughness significantly improve load-bearing capability, whereas porosity reduces it. Sangeetha et al. [29] explored MHD and viscosity variations effects on non-Newtonian fluids in porous triangular plates. Their results highlighted that viscosity variation enhances load capacity while reducing pressure under specific conditions. Sekar et al. [30] examined slip velocity with surface roughness and viscosity variation among porous, rough circular-shaped stepped surfaces using non-Newtonian fluids. Their findings emphasised improvements in load capacity due to roughness and viscosity variation.

Although extensive research has been conducted in the field of squeeze film lubrication, most existing studies have examined only a limited set of influencing parameters. For example, Lin et al. [31] explored how pressure-dependent viscosity affects couple stress fluids, reporting improvements in load-carrying capacity and longer film duration. Kumar and Sachidananda [32] studied the influence of surface roughness and viscosity variation in journal bearings, highlighting their combined effect on performance. Rajashekar and Kashinath [33] investigated MHD effects using a combination of couple stress theory and Christensen's stochastic roughness model for squeeze films between a sphere and a porous flat surface. Their results indicated that couple stress fluids enhance pressure and load-carrying capacity, with azimuthal roughness improving, and radial roughness diminishing, the film characteristics. Similarly, Baksh and Hanumagowda [34] analysed curved annular surfaces, demonstrating that magnetic fields and couple stress fluids can improve performance, with longitudinal and transverse roughness showing contrasting effects. However, these studies did not incorporate the full range of influential factors, namely viscosity variation, surface roughness, porosity, couple stress effects and magnetohydrodynamics into a single comprehensive model. As a result, the combined effect of these interacting factors remains largely unexplored. This gap is especially important for optimising lubrication systems in industries such as aerospace, automotive, biomedical devices and nanotechnology, where these combined effects significantly influence performance and durability.

To address existing limitations in the literature, the present study develops a comprehensive model that integrates all key influencing factors to provide a holistic understanding of squeeze film lubrication. Previous studies often examined effects such as viscosity variation, surface roughness, porosity, couple stress, and magnetohydrodynamics in isolation, resulting in an incomplete understanding of their combined influence. This work bridges that gap by introducing a unified approach supported by clearly defined research questions: How do viscosity variation, longitudinal and transverse surface roughness, porosity, couple stress and MHD forces collectively affect squeeze film characteristics such as pressure distribution, load-carrying capacity and squeeze film time? What are the distinct effects of longitudinal versus transverse roughness patterns on squeeze film characteristics? How can multi-parameter optimisation enhance the overall lubrication performance? And how is the proposed model validated for accuracy and reliability? These questions align with the study's objectives and guide a focused and coherent investigation. By integrating all major parameters into a single model, this research offers new insights into lubrication behaviour and performance. The findings contribute to the development of advanced lubrication systems and bearing designs, with practical relevance in fields such as MEMS, nanotechnology, rotating machinery and high-precision manufacturing, especially in applications involving micro- and nanoscale lubrication challenges.

2. Mathematical formulation

A cylinder with radius R is positioned above a rough, porous flat surface, with a homogeneous magnetic field B_0 employed along the x-axis. The cylinder and the flat porous plate are separated by a distance h. As the cylinder moves downward toward the plate with a velocity of V, a squeeze film effect is generated within the fluid region between them. The lubricant in this region is modelled as a couple stress fluid, which accounts for the microstructural interactions within the fluid. It is assumed that no external body forces or couples are acting on the system. The motion and continuity of the fluid are governed by the mathematical equations derived by Jyothi et al. [15], which provide the necessary framework for describing the behaviour of the

fluid in this configuration. The fundamental expression is represented as follows (see also Fig. 1):

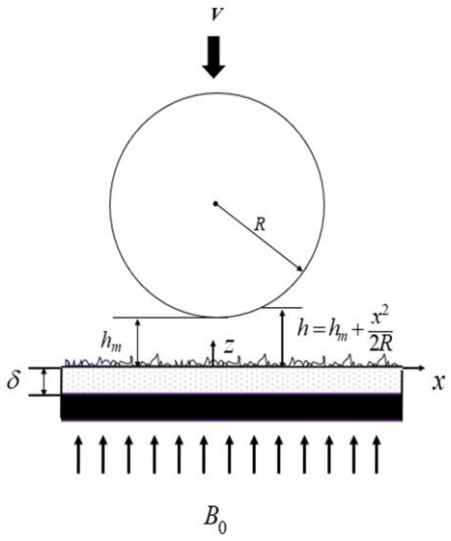

Fig. 1. The geometry of squeeze film lubrication between a cylinder and a rough porous flat surface.

$$\mu\frac{\partial^2 u}{\partial z^2}-\eta\frac{\partial^4 u}{\partial z^4}-\sigma B_0^2 u=\frac{\partial p}{\partial x}, \tag{1}$$

$$\frac{\partial u}{\partial x}+\frac{\partial w}{\partial z}=0, \tag{2}$$

$$\frac{\partial p}{\partial z}=0, \tag{3}$$

*w*hereby

$$M_0=B_0 h_{m_0}\left(\sigma/\mu\right)^{1/2}.$$

Darcy's law governing the porous area under the influence of MHD is given in a reduced form as follows:

$$u^*=\frac{-k}{\mu\left(1-\beta+\frac{k\sigma B_0^2}{\mu M}\right)}\frac{\partial p^*}{\partial x}, \tag{4}$$

$$w^*=\frac{-k}{\mu(1-\beta)}\frac{\partial p^*}{\partial z}. \tag{5}$$

Boundary conditions are:
- at the upper region $z = h$:

$$u=0,\qquad \frac{\partial^2 u}{\partial z^2}=0,\quad \text{and}\quad w=V=-\frac{\partial h}{\partial t}, \tag{6}$$

- at the lower region $z = 0$:

$$u=0,\qquad \frac{\partial^2 u}{\partial z^2}=0,\quad \text{and}\quad w=-w^*. \tag{7}$$

For the film region where x is less than R, the value of h is determined by:

$$h=h_m+\frac{x^2}{2R}.$$

By solving Eq. (1) and utilising the conditions (6−7), we obtain a solution for $u(x,z)$ as follows:

$$u(x,z)=\frac{1}{\sigma B_0^2}\frac{\partial p}{\partial x}\left[\frac{A^2}{A^2-B^2}\frac{\cosh\{B(2z-h)/2l\}}{\cosh(Bh/2l)}+\right.$$

$$\left.-\frac{B^2}{A^2-B^2}\frac{\cosh\left\{\frac{A(2z-h)}{2l}\right\}}{\cosh\left(\frac{Ah}{2l}\right)}-1\right]. \tag{8}$$

The condition discussed by Barus [35,36] as viscosity pressure dependency is described as follows:

$$\mu=\mu_0 e^{\alpha p}. \tag{9}$$

By substituting u from Eq. (8) into Eq. (2), integrating from 0 to h with the boundary conditions (6−7), and applying condition (9), we obtain a modified Reynolds expression:

$$\frac{\partial}{\partial x}\left\{\frac{e^{-\alpha p}}{\mu_0}g(h,l,M_0)\frac{\partial p}{\partial x}\right\}=V. \tag{10}$$

Here:

$$g(h,l,M_0)=\frac{h_{m_0}^2}{M_0^2}\left\{\frac{2l}{A^2-B^2}\left(\frac{B^2}{A}tanh\frac{Ah}{2l}-\frac{A^2}{B}tanh\frac{Bh}{2l}\right)+h\right\}+$$

$$+\frac{k\delta M_0^2}{h_{m_0}^2\left(1-\beta+\frac{kM_0^2}{h_{m_0}^2 m}\right)},$$

$$A=\left\{\frac{1+\left(1-{}^{4M_0^2l^2}/_{h_{m_0}^2}\right)^{1/2}}{2}\right\}^{1/2},$$

$$B=\left\{\frac{1-\left(1-{}^{4M_0^2l^2}/_{h_{m_0}^2}\right)^{1/2}}{2}\right\}^{1/2}.$$

The film thickness can be divided into two portions to create a mathematical model representing the surface's roughness.

$$H=h+h_s(x,z,\xi). \tag{11}$$

Considering the stochastic mean, Eq. (10) with respect to $g(h_s)$, we get:

$$\frac{\partial}{\partial x}\left\{\frac{e^{-\alpha E(p)}}{\mu_0}E\{g(H,l,M_0)\}\frac{\partial E(p)}{\partial x}\right\}=V, \tag{12}$$

where $E(*)=\int_{-\infty}^{\infty}(*)g(h_s)dh_s$.

The roughness function, as described by Christensen [2], is regarded as:

$$g(h_s)=\begin{cases}\frac{35}{32c^7}(c^2-h_s^2)^3, & -c<h_s<c\\ 0, & elsewhere\end{cases}, \tag{13}$$

where $c=3\bar{\sigma}$.

From Christensen's [2] perspective, it is employed to examine two distinct forms of one-dimensional roughness, such as longitudinal and transverse roughness patterns.

Longitudinal roughness patterns

The longitudinal roughness patterns have elongated, thin spikes and an inclined valley that runs along the x-axis. Subsequently:

$$H=h+h_s(z,\xi). \tag{14}$$

Transverse roughness patterns

The transverse roughness patterns have elongated, thin spikes and an inclined valley that runs along the *z*-axis. Subsequently:

$$H = h + h_s(x, \xi). \tag{15}$$

The average modified Reynolds flow equation is as follows:

$$\frac{\partial}{\partial x}\left\{\frac{e^{-\alpha E(p)}}{\mu_0} G(H, l, M_0, c)\frac{\partial E(p)}{\partial x}\right\} = V, \tag{16}$$

where:
- for longitudinal roughness:

$$G(H, l, M_0, c) = E[g(H, l, M_0)],$$

- for transverse roughness:

$$G(H, l, M_0, c) = E\left[1/g(H, l, M_0)\right].$$

Introducing dimensionless quantities as shown below:

$$x^* = \frac{x}{R}, \quad C = \frac{c}{h_{m_0}}, \quad h_m^* = \frac{h_m}{h_{m_0}}, \quad l^* = \frac{2l}{h_{m_0}},$$

$$P^* = -\frac{h_{m_0}^3 E(p)}{\mu_0 RV}, \quad \delta^* = \frac{\delta}{h_{m_0}}, \quad G = -\frac{\alpha \mu_0 RV}{h_{m_0}^2},$$

$$\beta = \frac{h_{m_0}}{R}, \quad h^* = \frac{h}{h_{m_0}} = h_m^* + \frac{x^{*2}}{2\beta}, \quad h_s^* = \frac{h_s}{h_{m_0}}, \quad \psi = \frac{k\delta}{h_{m_0}^3},$$

and substituting the specified dimensionless parameters into Eq. (16) yields:

$$\frac{d}{dx^*}\left\{e^{-GP^*} G^*(H^*, l^*, M_0, C, \psi)\frac{dP^*}{dx^*}\right\} = -\frac{1}{\beta}, \tag{17}$$

where:
- for longitudinal roughness:

$$G^*(H^*, l^*, M_0, C, \psi) = E[g^*(H^*, l^*, M_0, \psi)],$$

- for transverse roughness:

$$G^*(H^*, l^*, M_0, C, \psi) = E\left[1/g^*(H^*, l^*, M_0, \psi)\right],$$

$$E[g^*(H^*, l^*, M_0, \psi)] =$$

$$= \frac{35}{32c^7}\int_{-C}^{C} g^*(H^*, l^*, M_0, \psi)\,(c^2 - h_s^{*2})^3 dh_s^*,$$

$$E\left[1/g^*(H^*, l^*, M_0, \psi)\right] = \frac{35}{32c^7}\int_{-C}^{C} \frac{(c^2 - h_s^{*2})^3}{g^*(H^*, l^*, M_0, \psi)} dh_s^*,$$

$$g^*(H^*, l^*, M_0, \psi) =$$

$$= \frac{1}{M_0^2}\left\{\frac{l^*}{A^{*2} - B^{*2}}\left(\frac{B^{*2}}{A^*} tanh\frac{A^* H^*}{l^*} - \frac{A^{*2}}{B^*} tanh\frac{B^* H^*}{l^*}\right) + H^*\right\} +$$

$$+ \frac{\psi M_0^2}{\left(1 - \beta + \frac{\psi M_0^2}{\delta^* m}\right)},$$

$$A^* = \left\{\frac{1 + \sqrt{1 - (l^* M_0)^2}}{2}\right\}^{1/2},$$

$$B^* = \left\{\frac{1 - \sqrt{1 - (l^* M_0)^2}}{2}\right\}^{1/2}.$$

The following are the pressure boundary conditions:

$$\frac{dP^*}{dx^*} = 0 \text{ at } x^* = 0, \tag{18}$$

$$P^* = 0 \text{ at } x^* = 1. \tag{19}$$

By solving Eq. (17) and incorporating Eqs. (18−19), we get:

$$P^* = -\frac{1}{G} ln\left\{1 + \frac{1}{\beta}\int_1^{x^*} \frac{Gx^*}{G^*(H^*, l^*, M_0, C, \psi)} dx^*\right\}. \tag{20}$$

The load-bearing capacity is:

$$W = D\int_{-R}^{R} p dr.$$

The non-dimensional load-carrying capability is:

$$W^* = \frac{W h_{m_0}^3}{\mu_0 R^2\left(\frac{dh}{dt}\right)} =$$

$$= -\frac{1}{G}\int_{-1}^{1}\left[ln\left\{1 + \frac{1}{\beta}\int_1^{x^*} \frac{Gx^*}{G^*(H^*, l^*, M_0, C, \psi)} dx^*\right\}\right] D\, dx^*. \tag{21}$$

The dimensionless time is attained by integrating Eq. (21):

$$T^* = \frac{t h_{m_0}^2}{B\mu_0 R^2} =$$

$$= -\frac{1}{G}\int_{h_1^*}^{1}\left\langle\int_{-1}^{1}\left[ln\left\{1 + \frac{1}{\beta}\int_1^{x^*} \frac{Gx^*}{G^*(H^*, l^*, M_0, C, \psi)} dx^*\right\}\right] D\, dx^*\right\rangle dh_m^*. \tag{22}$$

3. Methodology

This study investigates squeeze film lubrication between a cylinder and a rough, porous flat surface through a comprehensive theoretical and numerical methodology, integrating multiple physical phenomena into a unified model. The lubricant, modelled as a couple stress fluid using Stokes' theory, is assumed to exhibit isothermal, incompressible flow without external body forces or couples, with pressure-dependent viscosity governed by Barus' law. Surface roughness is characterised via Christensen's stochastic model for longitudinal and transverse patterns, and porosity is incorporated using Darcy's law. The governing equations of motion and continuity are solved under appropriate boundary conditions to derive a velocity field, leading to a modified Reynolds equation that integrates roughness effects and magnetohydrodynamic influences via the Hartmann number. The model is non-dimensionalised for the generalised analysis, yielding dimensionless pressure distributions, and analytical expressions for load-carrying capacity and squeeze film time are established where feasible. Solving the modified Reynolds equation is not merely a mathematical exercise, but a crucial step that enables accurate prediction of lubrication performance under complex conditions. This understanding is essential for optimising system design in high-precision applications, including advanced manufacturing. To address the complexity of interdependent parameters (Hartmann number, surface roughness, viscosity variation, couple stress and porosity), the lubrication domain is discretised with a uniform rectangular mesh, optimised through convergence studies for computational accuracy. Numerical integration is performed using Simpson's one-third rule, which is well-suited for capturing the smooth variations inherent in the system. This numerical approach not only demonstrates

the capability to solve the modified Reynolds equation but also provides practical benefits by enabling detailed analysis of lubrication performance across a wide range of operating conditions. Comprehensive data collection is achieved through systematic simulations across a wide range of realistic parameter values: surface roughness (C = 0, 0.3, 0.5), viscosity variation (G = 0.001, 0.003, 0.005), couple stress parameter (l^* = 0, 0.2, 0.4), Hartmann number (M_0 = 0, 2, 4), and porosity (ψ = 0.001, 0.002, 0.004). Other parameters are held constant at m = 0.1, α = 0.2, δ = 0.1, h_m^* = 0.8, and β = 0.04. For each parameter combination, simulations are performed to compute the pressure distribution, load-carrying capacity and squeeze film time. The simulation results are presented in tabular form and visualised through 2D and 3D plots to illustrate parameter sensitivity, interdependencies and performance trends. The interpretation emphasises both the magnitude and direction of each parameter's effect on lubrication performance, ensuring the derivation of meaningful engineering insights. Then, error analysis is conducted by comparing numerical results with analytical solutions, achieving strong agreement with relative errors typically below a very small percentage, confirming the model's robustness. Discrepancies are quantified using standard metrics such as mean absolute error to ensure reliability. Finally, the model's validity is confirmed by comparing numerical results with analytical solutions, showing strong agreement. Crucially, unlike previous studies, which often analysed parameters in isolation (e.g. Lin et al. [31]), this methodology integrates all relevant physical factors – couple stress, roughness, porosity and viscosity variation – within a single cohesive framework, providing a more accurate and holistic understanding of lubrication performance for enhanced predictive capabilities in aerospace, biomedical, and micro/nano-scale applications.

4. Results and discussion

This study examines how surface roughness (C), viscosity changes (G), couple stress (l^*), Hartmann number (M_0) and porosity (ψ) affect squeeze film lubrication performance, focusing on dimensionless pressure (P^*), load carrying capacity (W^*) and squeeze film time (T^*). By solving governing equations, we understand how these factors impact fluid flow, helping to optimise lubrication systems for better efficiency and durability in engineering fields like bearings and seals in the automotive and aerospace industries. This detailed parametric analysis, which explores the interaction of various factors, sets this work apart from previous studies and offers practical design recommendations.

4.1. Pressure

The plot of P^* with x^* for various C, with α = 0.2, M_0 = 2, l^* = 0.4, ψ = 0.001, β = 0.04, h_m^* = 0.8, G = 0.002, δ = 0.1 and m = 0.1 is displayed in Fig. 2. It is witnessed that the configuration of the one-dimensional roughness pattern coincides at C = 0, indicating no pressure variation. As C increases, irregularities in the surface lead to higher flow resistance, resulting in less effective pressure forces in the flow direction. Consequently, P^* declines for the longitudinal roughness pattern. This is because higher roughness increases friction and impedes fluid flow, leading to a diminished pressure. In contrast, the transverse roughness pattern enhances P^* as C rises, as the fluid interacts with additional obstacles or irregularities perpendicular to the flow direction, enhancing the pressure.

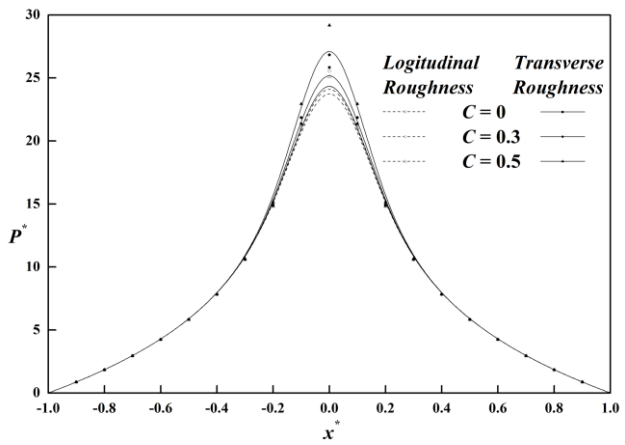

Fig. 2. Plot of P^* versus x^* for different C.

In Fig. 3, P^* vs. x^* for different M_0 is illustrated, with α = 0.2, m = 0.1,h_m^* = 0.8, G = 0.002, C = 0.3, δ = 0.1, ψ = 0.001, l^*=0.4 and β = 0.04. It is revealed that as M_0 enhances, the influence of MHD stabilises the fluid flow through surface irregularities, resulting in enhanced P^*. This stabilisation reduces turbulence and allows the fluid to navigate irregularities more efficiently, leading to a higher pressure.

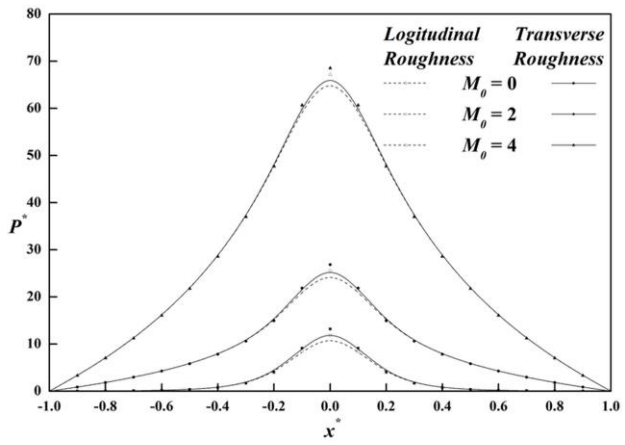

Fig. 3. Plot of P^* with respect to x^* for different M_0.

Figure 4 shows the plot of P^* against x^* for distinct l^*. It is noticed that as l^* increases, there is increased fluid restriction within the roughness region, leading to an enhancement in pressure P^*. Higher couple stress results in greater fluid resistance to deformation, which improves the pressure by causing the fluid to exert more force against the rough surfaces.

In Fig. 5, P^* versus x^* for different ψ is presented. It is observed that increasing ψ improves fluid absorption through the porous regions. However, the delay of flow due to pores reduces the capacity of fluids to establish pressure within the surfaces,

resulting in a decline in pressure as the fluid's pressure is compromised by the delayed flow through the porous medium.

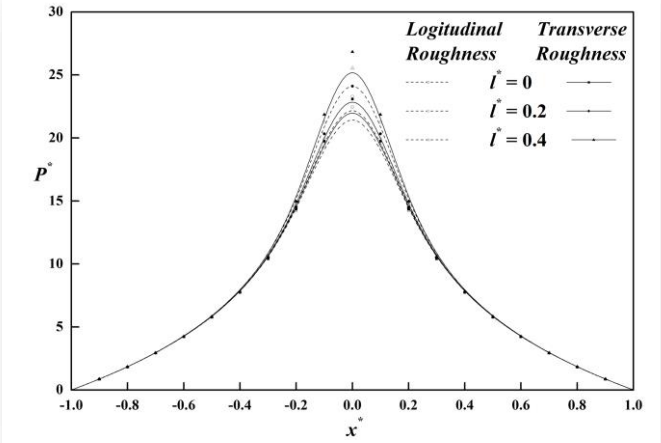

Fig. 4. Graph of P^* versus x^* for various l^*.

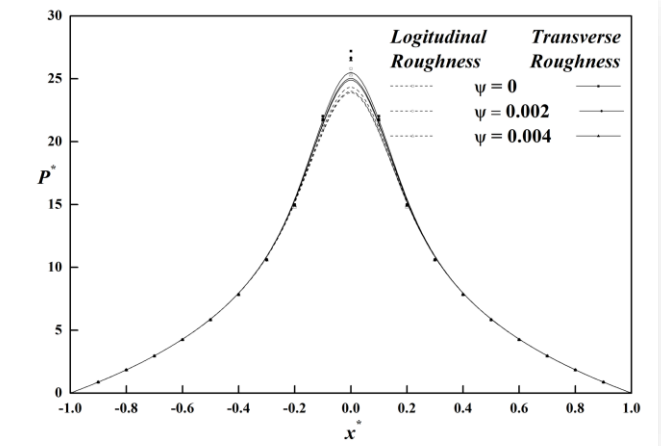

Fig. 5. Plot of P^* versus x^* for different ψ.

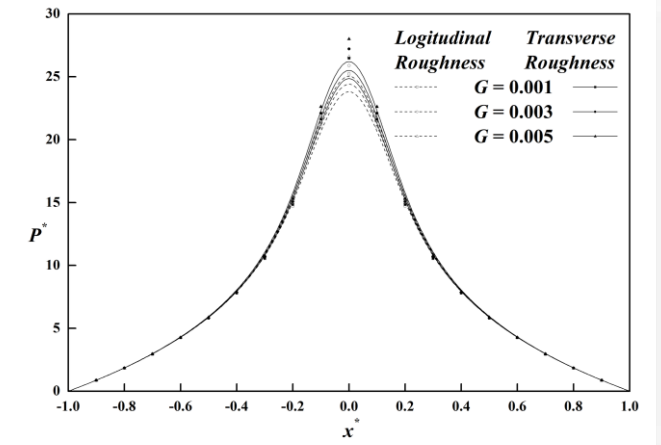

Fig. 6. Plot of P^* versus x^* for various G.

The function P^* against x^* for distinct G is shown in Fig. 6. It is revealed that as G rises, P^* also enhances due to changes in fluid behaviour. Higher viscosity variation makes the fluid more resistant to flow changes, which helps maintain pressure within the squeeze film by better managing the fluid's interaction with surface irregularities. Overall, the observed variations in pressure profiles can be linked to how surface roughness, magnetic fields, fluid restrictions, porosity and viscosity affect fluid dynamics. Smoother surfaces, magnetic stabilisation and higher couple stress generally enhance pressure, while increased roughness, higher porosity and viscosity variations can either improve or impede pressure depending on their specific effects on fluid flow and interaction with the surface. These insights are valuable for designing more efficient lubrication systems in engineering applications, where maintaining optimal pressure and flow characteristics is crucial.

4.2. Load-carrying capacity

The graph of W^* versus h_m^* for distinct C, with G = 0.002, ψ = 0.001, M_0 = 2, β = 0.04, l^*=0.4, α = 0.2, δ = 0.1, m = 0.1, is presented in Fig. 7.

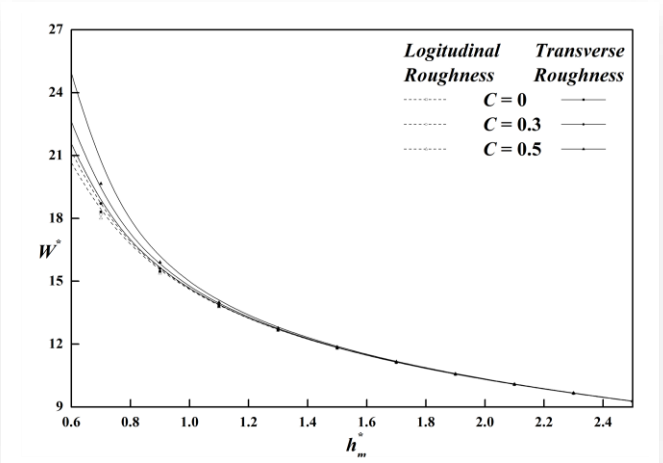

Fig. 7. Graph of W^* versus h_m^* for different C.

It is noticed that at C = 0, the configuration of the one-dimensional roughness pattern coincides. Moreover, as the C enhances, W^* declines for the longitudinal roughness pattern due to increased surface interactions, resulting in higher friction and reduced efficiency in load-bearing capacity. The rougher surface increases resistance, diminishing the film's load-carrying capacity. Conversely, W^* enhances as C rises for the transverse roughness pattern. The increased surface roughness enhances fluid interaction vertical to the flow direction, improving the film's ability to support loads by increasing fluid retention and film stability.

Figures 8 and 9 depict W^* vs. h_m^* for distinct M_0 and l^*, with α = 0.2, β = 0.04, G = 0.002, δ = 0.1, C = 0.3, and ψ = 0.001. It is found that as M_0 and l^* increase, fluid behaviour becomes more responsive to the magnetic field and couple stress. This enhanced responsiveness leads to improved fluid confinement within the roughness regions, which enhances W^*. The magnetic field and couple stress increase the fluid's resistance to distortion and stabilise its flow, allowing for better load support within the film.

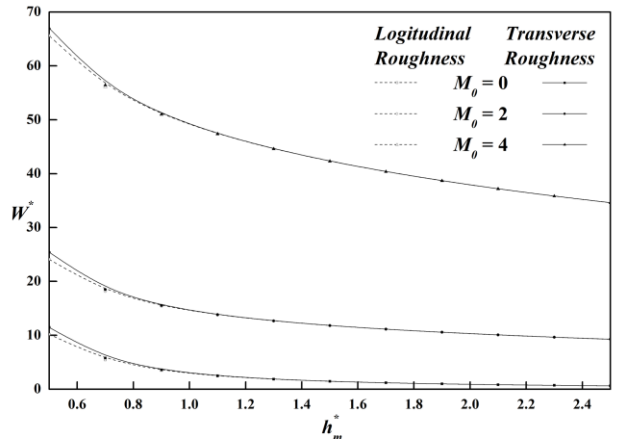

Fig. 8. Graph of W^* versus h_m^* for different M_0.

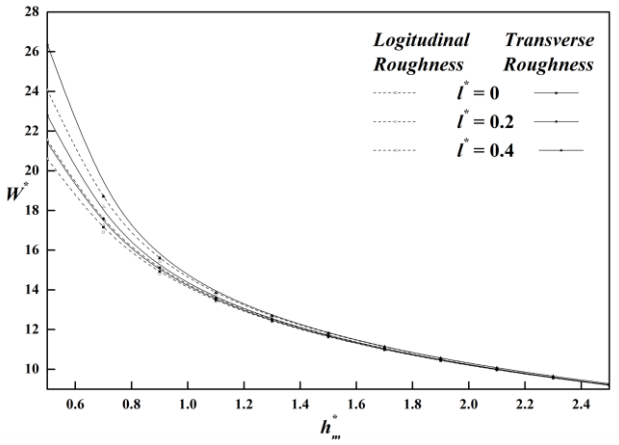

Fig. 9. Plot of W^* with h_m^* for distinct l^*.

Figure 10 demonstrates W^* against h_m^* for different ψ, with $M_0 = 2$, $\alpha = 0.2$, l^*=0.4, $m = 0.1$, $G = 0.002$, $C = 0.3$, $\beta = 0.04$, and $\delta = 0.1$. It is noticed that as ψ enhances, fluid penetration through porous regions enhances, but this enhanced fluid absorption results in reduced load-bearing capacity. The increased porosity delays fluid flow and decreases the film's ability to establish and maintain effective pressure, leading to a decrease in W^*.

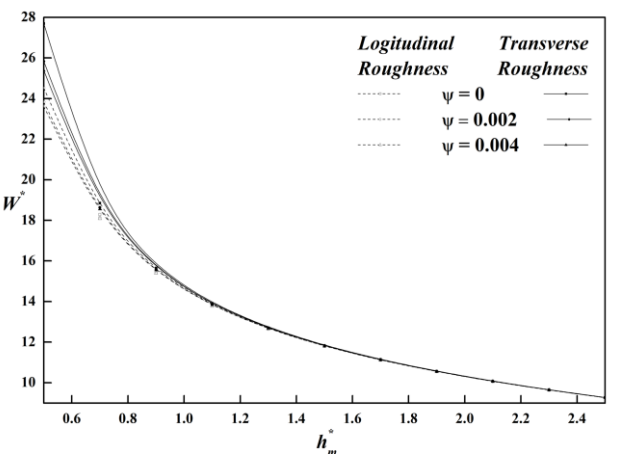

Fig. 10. Graph of W^* versus h_m^* for different ψ.

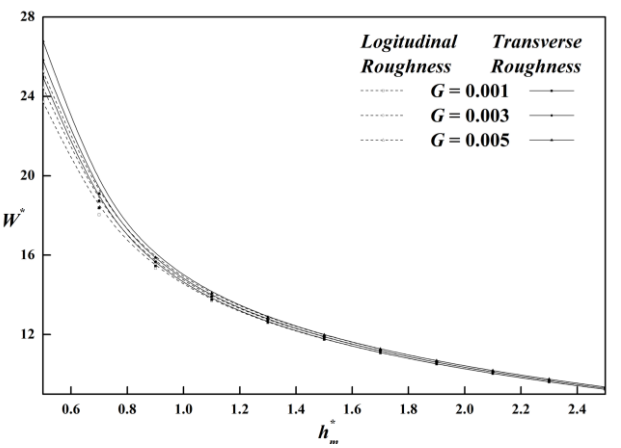

Figure 11. Graph of W^* versus h_m^* for different G.

The function W^* against h_m^* for different G is displayed in Fig. 11. It is seen that as G improves, W^* also improves. Higher viscosity variation alters fluid behaviour, enhancing its resistance to flow changes and increasing the fluid's load-bearing capability. This change helps the fluid maintain its support and stability within the roughness regions, leading to an improvement in W^*. In summary, the variations in W^* are linked to how roughness, magnetic fields, couple stress, porosity and viscosity affect fluid dynamics within the squeeze film. Increased roughness in the longitudinal direction generally decreases load-bearing capacity due to higher friction, while transverse roughness can improve it by enhancing fluid support. Magnetic fields and couple stress improve fluid confinement and load support, higher porosity reduces the film's load-bearing capacity, and increased viscosity variation stabilises fluid behaviour, thereby enhancing load support. These findings are crucial for optimising lubrication systems and designing effective bearing surfaces in engineering applications.

4.3. Squeeze film time

Figure 12 illustrates the graph of T^* vs. h_m^* for various C, with $\psi = 0.001$, $G = 0.002$, $M_0 = 2$, l^*=0.4, $\delta = 0.1$, $m = 0.1$, $\alpha = 0.2$, $\beta = 0.04$, $G = 0.002$. It is noted that at $C = 0$, the configuration of the one-dimensional roughness pattern coincides. Moreover, as C rises, T^* declines for the longitudinal roughness pattern. This decline is due to increased fluid permeation through the rough surface, which reduces the film's ability to sustain a longer squeeze time. Conversely, T^* increases for the transverse roughness pattern as C rises. In this case, the roughness enhances fluid confinement and retention, which prolongs the squeeze film time by improving the stability and duration of the fluid layer.

Figures 13 and 14 depict the function T^* vs. h_m^* for distinct M_0 and l^*, with $\delta = 0.1$, $\psi = 0.001$, $G = 0.002$, $C = 0.3$, $m = 0.1$, $\beta = 0.04$, $\alpha = 0.2$. It is found that as M_0 and l^* increase, fluid motion becomes more responsive to the magnetic field and couple stress, leading to improved fluid containment within the roughness regions. This results in an increase in T^*, as the enhanced fluid behaviour supports a longer film duration.

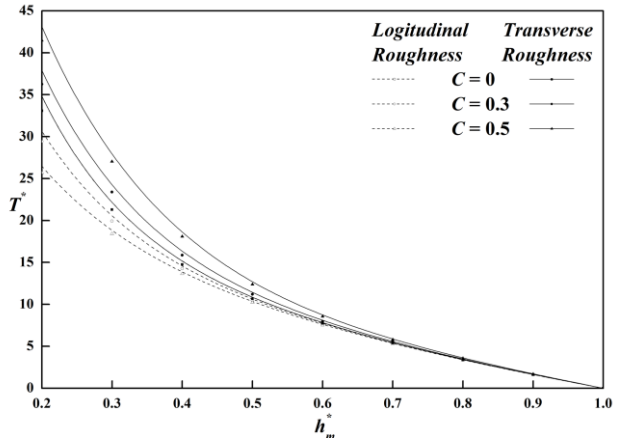

Fig. 12. T^* with h_m^* for various C.

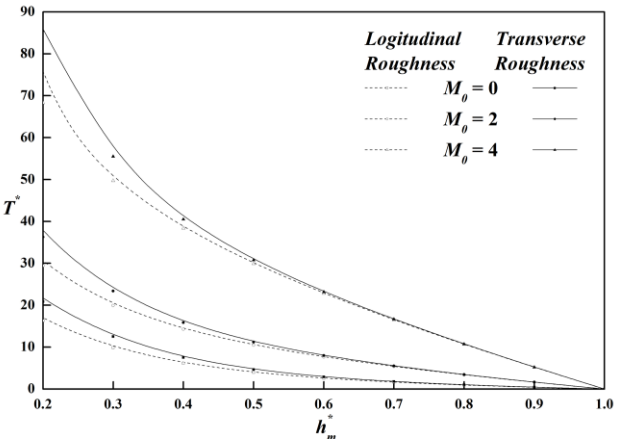

Fig. 13. T^* with h_m^* for various M_0.

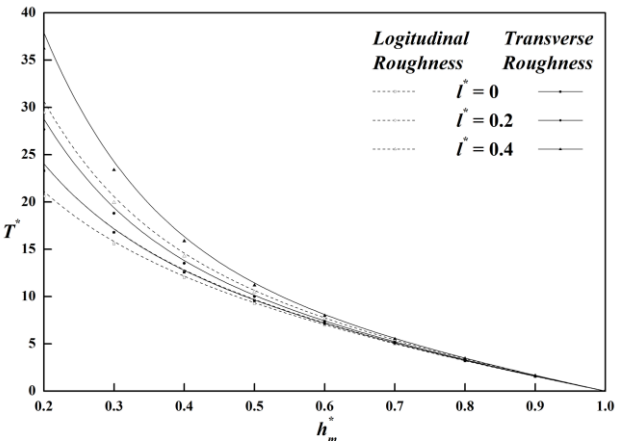

Fig. 14. T^* with h_m^* for different l^*.

The graph of T^* versus h_m for various ψ is presented in Fig. 15, with $\alpha = 0.2$, $l^*=0.4$, $m = 0.1$, $C = 0.3$, $\delta = 0.1$, $\beta = 0.04$, $G = 0.002$, $M_0 = 2$. It is shown that as ψ rises, higher porosity reduces the fluid's ability to remain contained within the film. The increased porosity allows more fluid to escape through the porous regions, leading to a decrease in T^* as the fluid's ability to maintain a stable film is diminished.

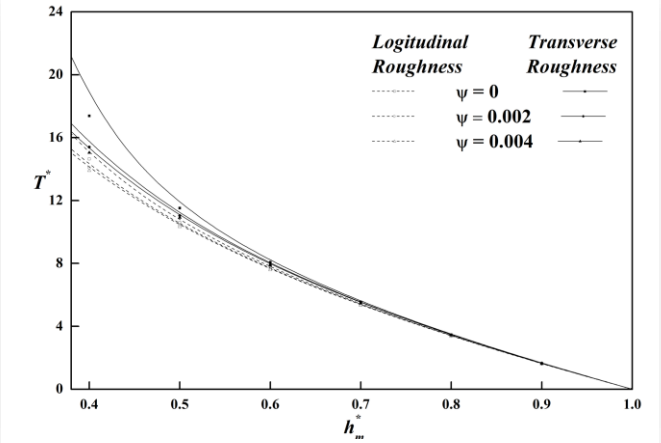

Fig. 15. T^* with h_m^* for different ψ.

Figure 16 describes T^* changing with h_m^* for different G, showing that T^* enhances as G rises. Higher viscosity variation alters the fluid's behaviour, enhancing its resistance to flow changes and improving its ability to remain within the film for a longer period. These consequences occur in an extended squeeze film time, as the fluid's stability is better maintained despite changes in surface roughness.

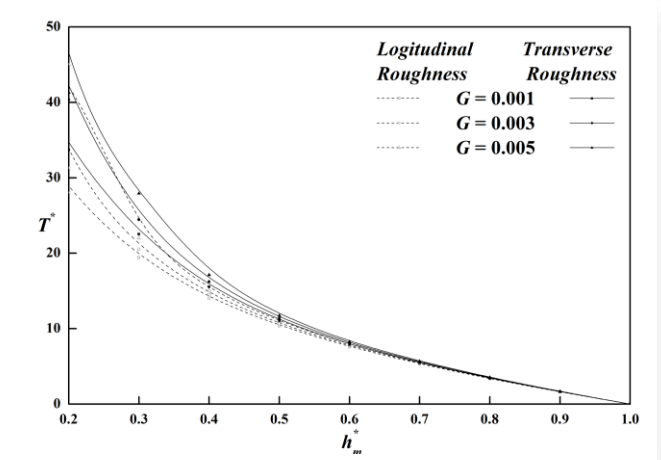

Fig. 16. T^* versus h_m^* for various G.

Overall, the observed variations in T^* are related to how different factors affect fluid behaviour within the squeeze film. Increased roughness in the longitudinal direction leads to reduced squeeze film time due to greater fluid permeation, while transverse roughness improves fluid retention and prolongs squeeze time. Enhanced magnetic fields and couple stress, along with higher viscosity variation, contribute to improved fluid stability and extended squeeze time, whereas higher porosity diminishes the film's ability to sustain a longer film duration. These findings are crucial for designing lubrication systems where maintaining optimal squeeze film time is essential for reliable performance.

4.4. Combined effect of roughness and porosity, viscosity variation, Hartmann number and couple stress

To comprehensively evaluate the interdependence of parameters affecting squeeze film performance, this section presents an extensive three-dimensional parametric analysis examining the combined effects of surface roughness with porosity, viscosity variation, Hartmann number and couple stress parameter on the dimensionless pressure, load-carrying capacity and squeeze film time. The study considers both longitudinal and transverse roughness patterns, revealing complex interactions that provide valuable insights for optimising lubrication system performance. To enhance clarity and address the need for varied graphical representation, three-dimensional surface plots are utilised. The results are further contextualised with practical applications in engineering domains that demand precise fluid dynamic control.

4.4.1. Combined effect of roughness and porosity

Figures 17−22 present the three-dimensional interaction between surface roughness and porosity on dimensionless pressure, load-carrying capacity and squeeze film time, under both longitudinal and transverse roughness configurations. The analysis was performed using the parameters: M_0 = 1, G = 0.04, h_m* = 0.7, α = 0.2, l* = 0.3, δ = 0.1, m = 0.1, and β = 0.3. For longitudinal roughness, the results reveal that a simultaneous reduction in roughness pattern and porosity leads to a significant enhancement in all three performance indicators: P*, W* and T*. This suggests that smoother surfaces, coupled with lower fluid absorption through the porous structure, facilitate more effective pressure build-up and stronger load-bearing capabilities. From a lubrication design perspective, this combination minimises energy losses due to flow resistance and ensures prolonged squeeze film support, which is essential for high-precision applications such as aerospace bearings and engine liners. On the other hand, under transverse roughness conditions, a different trend emerges. An increase in surface roughness combined with a decrease in porosity results in a corresponding improvement in pressure, load carrying capacity and squeeze film duration. This can be attributed to the transverse orientation introducing flow-interrupting features that trap the lubricant more efficiently. As the porosity decreases, less fluid is lost through absorption, allowing for a thicker, more stable film. This behaviour is particularly advantageous in industrial settings where components are exposed to heavy loads or intermittent shocks, such as in heavy-duty gears or piston-cylinder arrangements.

Overall, the combined effect of C and ψ highlights a dual design strategy: reducing both parameters under longitudinal roughness improves efficiency by reducing flow resistance, while increasing roughness under transverse configurations enhances lubricant retention and structural support. This duality underscores the importance of tailoring surface geometry and material porosity according to the orientation of the roughness pattern and specific operational demands. These findings not only contribute to the theoretical understanding of textured porous bearings but also provide a robust design framework for optimising tribological performance across a range of real-world applications.

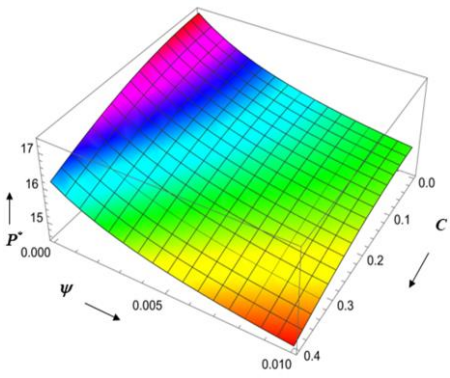

Fig. 17. P* vs. C (longitudinal roughness) and ψ.

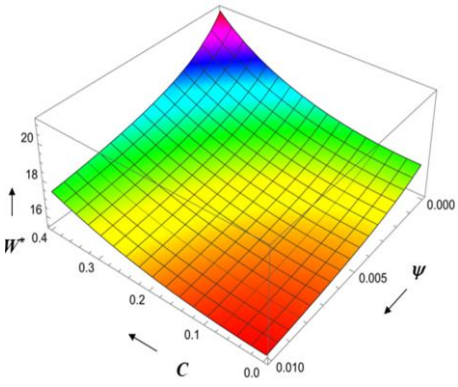

Fig. 18. W* vs. C (longitudinal roughness) and ψ.

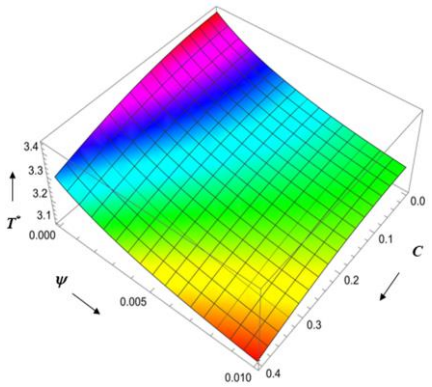

Fig. 19. T* vs. C (longitudinal roughness) and ψ.

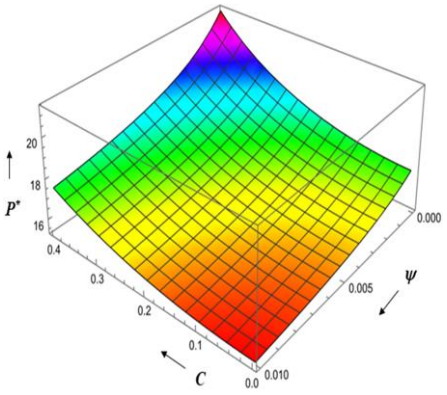

Fig. 20. P* vs. C (transverse roughness) and ψ.

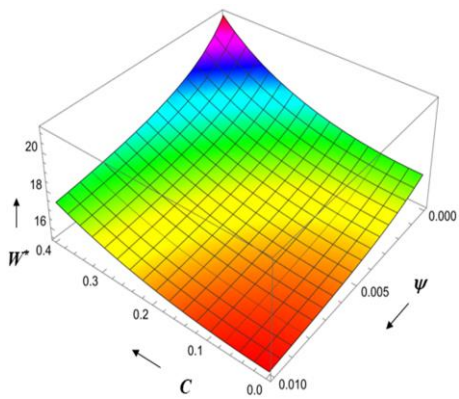

Fig. 21. W* vs. C (transverse roughness) and ψ.

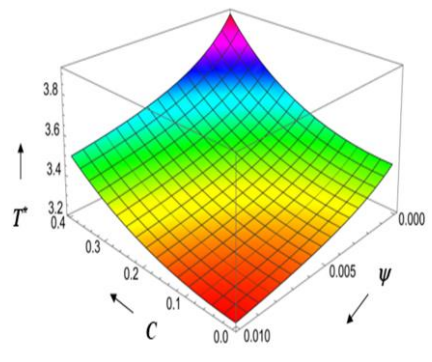

Fig. 22. T* vs. C (transverse roughness) and ψ.

4.4.2. Combined effect of roughness and viscosity variation

Figures 23−28 provide a comprehensive three-dimensional analysis of how the combined influence of surface roughness and viscosity variation affects P^*, W^* and T^*. The simulations are conducted using the following parameters: $m = 0.1$, $M_0 = 1$, $l^* = 0.3$, $\beta = 0.3$, $h_m^* = 0.7$, $\alpha = 0.2$, $\psi = 0.001$ and $\delta = 0.1$. For longitudinal roughness patterns, the results clearly show that a decrease in roughness combined with an increase in viscosity variation leads to significant improvements in P^*, W^* and T^*. This behaviour is physically intuitive: smoother surfaces reduce mechanical friction and irregularities that disrupt fluid flow, while enhanced viscosity variation improves the lubricant's resistance to shear deformation and allows it to better conform to surface features. The resulting increase in pressure and load-carrying capability, coupled with an extended squeeze film time, makes this combination highly advantageous in applications where maintaining a continuous and stable lubrication layer is critical, such as in precision mechanical systems, microbearings, and journal bearings in automotive and aerospace sectors. In contrast, for transverse roughness patterns, the study reveals that simultaneous increases in both C and G produce optimal performance. Unlike longitudinal patterns, transverse roughness introduces geometric features perpendicular to the flow direction, creating zones of increased fluid entrapment. When combined with higher viscosity variation, the fluid exhibits greater resistance to motion, while being retained more effectively between the rough textures. This synergy leads to improved pressure distribution, greater film thickness and prolonged film stability. Such behaviour is especially valuable in high-load, high-friction environments—such as heavy-duty gear systems, off-road vehicle suspensions and industrial press components—where maintaining lubricant integrity under variable stress conditions is essential.

Overall, the results highlight the nonlinear interplay between surface topography and fluid rheology, demonstrating that optimal performance is not solely dependent on minimising roughness or maximising viscosity variation but rather on the appropriate pairing of both based on surface orientation. For longitudinal roughness, smoother surfaces benefit more from increased viscosity gradients, while transverse configurations leverage roughness to trap and stabilise high-viscosity fluids. These findings contribute meaningful insights into the design of advanced lubrication systems, offering guidance on how to strategically manipulate surface and fluid parameters to improve tribological performance across diverse engineering applications.

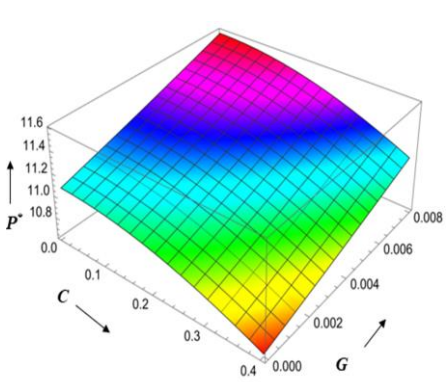

Fig. 23. P^* vs. C (longitudinal roughness) and G.

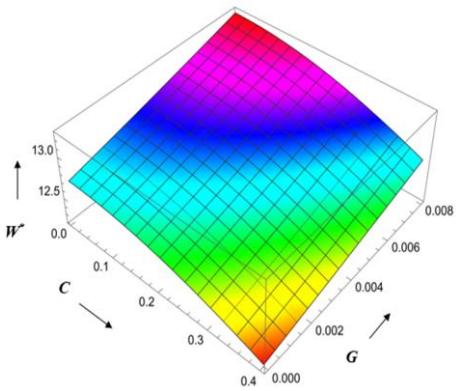

Fig. 24. W^* vs. C (longitudinal roughness) and G.

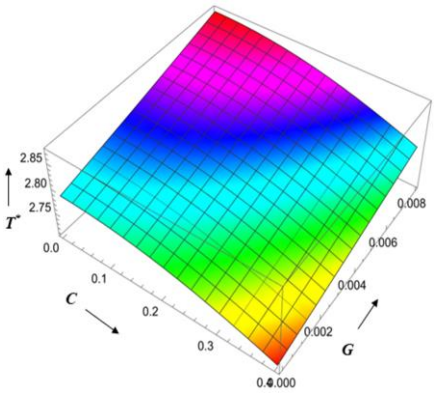

Fig. 25. T^* vs. C (longitudinal roughness) and G.

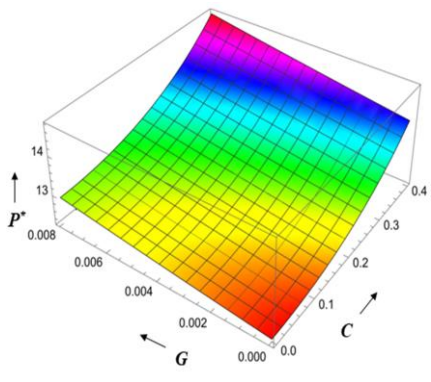

Fig. 26. P^* vs. C (transverse roughness) and G.

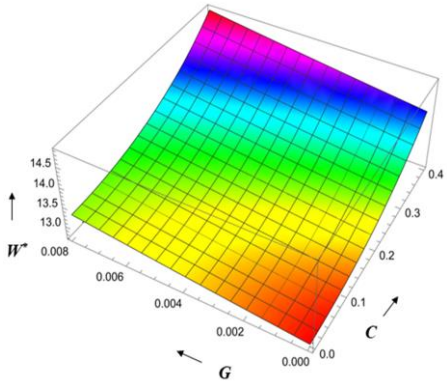

Fig. 27. W^* vs. C (transverse roughness) and G.

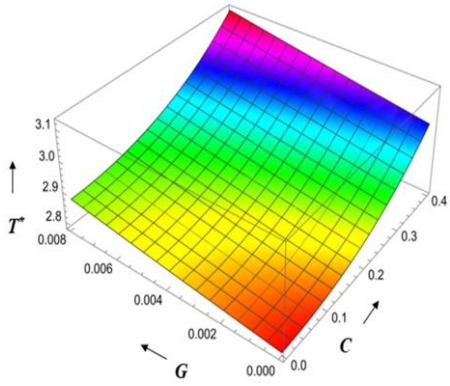

Fig. 28. T^* vs. C (transverse roughness) and G.

4.4.3. Combined effect of roughness and Hartmann number

Figures 29−34 illustrate the combined influence of surface roughness and Hartmann number on P^*, W^* and T^*. The simulations are conducted using the following fixed parameters: $\psi = 0.001$, $\beta = 0.3$, $G = 0.04$, $h_m^* = 0.7$, $l^* = 0.3$, $\alpha = 0.2$, $\delta = 0.1$ and $m = 0.1$. In the case of longitudinal roughness, the results reveal that decreasing surface roughness while increasing the Hartmann number yields pronounced improvements in all three performance indicators: P^*, W^* and T^*. The enhancement in

performance can be attributed to the MHD effect, where the application of a magnetic field induces Lorentz forces within the conductive fluid. These forces act to dampen velocity gradients, reduce turbulence and align fluid motion, thereby stabilising the flow through irregular rough regions. As a result, the fluid film becomes more resilient, better able to maintain pressure and capable of supporting higher loads over longer durations. This mechanism is particularly beneficial in lubrication systems involving magnetorheological or ferrofluid lubricants, where external magnetic fields can be strategically employed to enhance operational efficiency and reduce mechanical wear. For transverse roughness patterns, a different trend emerges. The data show that simultaneously increasing both roughness and Hartmann number leads to optimal performance. The underlying physics can be explained by the unique role of transverse roughness in introducing geometric barriers perpendicular to the flow. When combined with a strong magnetic field, these barriers enhance the retention of the fluid within the microcavities of the surface. The magnetic field dampens fluid motion in regions where escape is likely, improving fluid stability and resistance to leakage. Consequently, the lubricant film exhibits higher pressure and greater durability, which translates to increased load-bearing capacity and prolonged squeeze film time. From a practical standpoint, these results have significant engineering implications. In applications where magnetic fields can be externally controlled – such as in magnetorheological dampers, electric actuators and aerospace bearing systems – the deliberate tuning of surface roughness and magnetic intensity offers a valuable tool for real-time control of lubricant film behaviour. For longitudinal surfaces, smoothness should be prioritised alongside MHD effects to minimise friction and improve responsiveness. Conversely, for transverse patterns, enhanced surface roughness can be leveraged to synergise with magnetic stabilisation, ensuring film integrity even under dynamic and harsh operating conditions. Overall, the combined effect of roughness and Hartmann number illustrates the importance of aligning fluid control strategies with surface design. The MHD effect not only stabilises the fluid flow but also amplifies the positive or negative effects of roughness depending on its orientation. These findings bridge the gap between theoretical modelling and field applications, offering actionable insights for optimising lubrication systems in magnetically active environments.

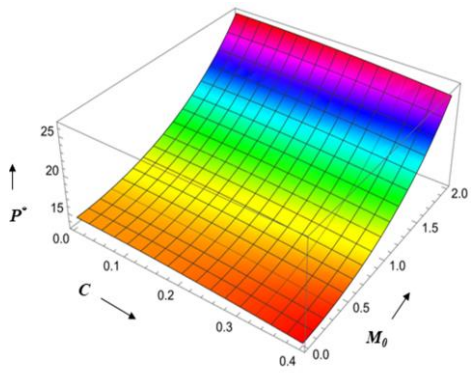

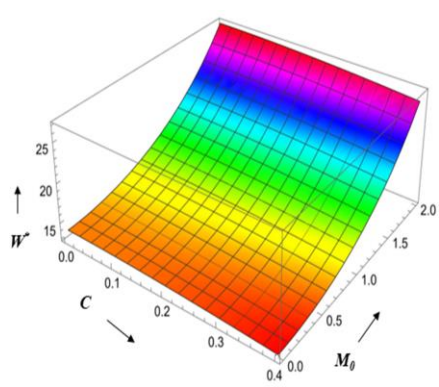

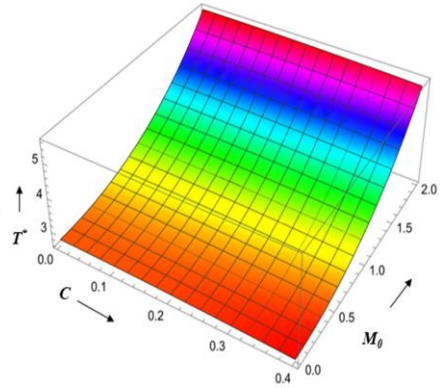

Fig. 29. P^* vs. C (longitudinal roughness) and M_0. Fig. 30. W^* vs. C (longitudinal roughness) and M_0. Fig. 31. T^* vs. C (longitudinal roughness) and M_0.

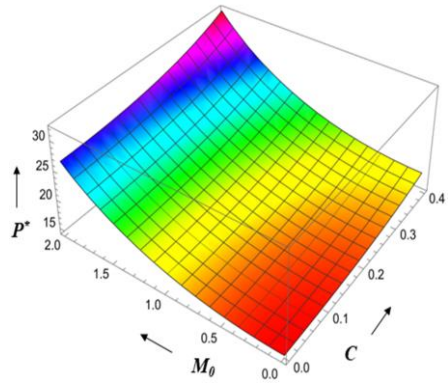

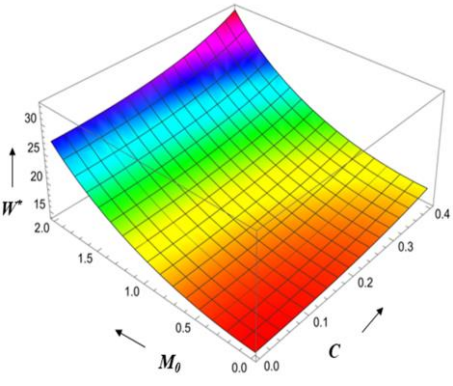

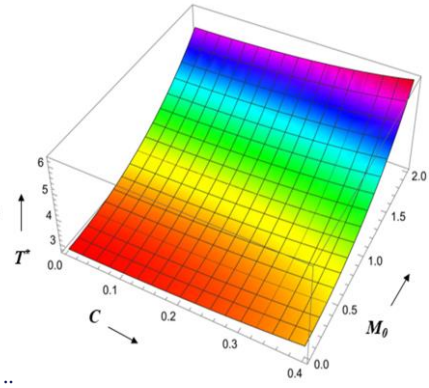

Fig. 32. P^* vs. C (transverse roughness) and M_0. Fig. 33. W^* vs. C (transverse roughness) and M_0. Fig. 34. T^* vs. C (transverse roughness) and M_0.

4.4.4. Combined effect of roughness and couple stress

Figures 35−40 present the combined influence of the surface roughness parameter and the couple stress parameter on the P^*, W^* and T^*, under the conditions: $G = 0.04$, $\beta = 0.3$, $M_0 = 1$, $\psi = 0.001$, $h_m^* = 0.7$, $\alpha = 0.2$, $\delta = 0.1$ and $m = 0.1$. The analysis is conducted for both longitudinal and transverse roughness patterns to uncover nuanced behaviours in complex fluid-structure interactions. For longitudinal roughness configurations, the study reveals that a decrease in surface roughness, when accompanied by an increase in the couple stress parameter, significantly enhances P^*, W^* and T^*. This trend can be attributed to the nature of couple stress fluids, which incorporate microstructural effects that resist velocity gradients and shear deformation. An elevated l^* value signifies stronger internal resistance within the fluid due to the presence of suspended particles, additives or

molecular chain entanglements. These microstructural effects stabilise the film, improve fluid retention and resist squeeze-induced thinning, ultimately resulting in higher pressure build-up and prolonged film duration. In contrast, under transverse roughness conditions, the combined increase of both C and l^* leads to noticeable improvements in performance. This synergy likely stems from the transverse roughness acting as a micro-reservoir system that works in tandem with the couple stress properties of the fluid. The enhanced surface texture traps the fluid more effectively, while the couple stress interactions prevent its rapid deformation or escape. As a result, the squeeze film remains stable over extended periods, even under cyclic or impact loading. This outcome is particularly relevant in high-load, high-frequency environments such as those found in microelectromechanical systems (MEMS), aerospace bearings and biomedical implants.

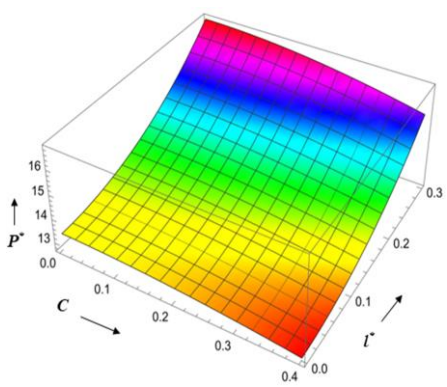

Fig. 35. P^* vs. C (longitudinal roughness) l^*.

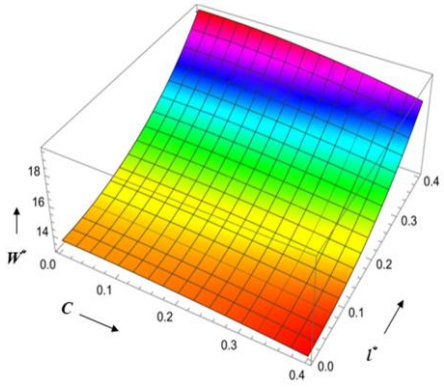

Fig. 36. W^* vs. C (longitudinal roughness) and l^*.

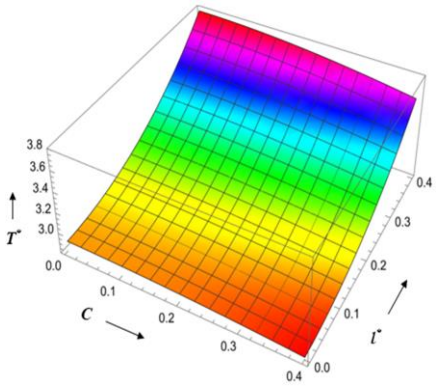

Fig. 37. T^* vs. C (longitudinal roughness) and l^*.

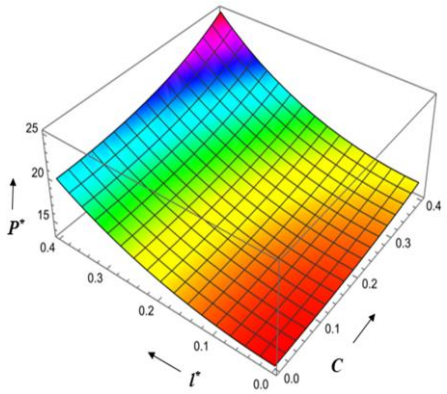

Fig. 38. P^* vs. C (transverse roughness) and l^*.

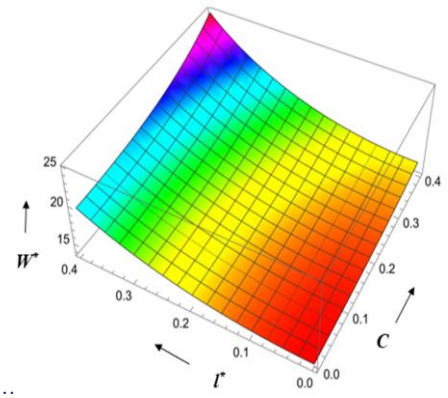

Fig. 39. W^* vs. C (transverse roughness) and l^*.

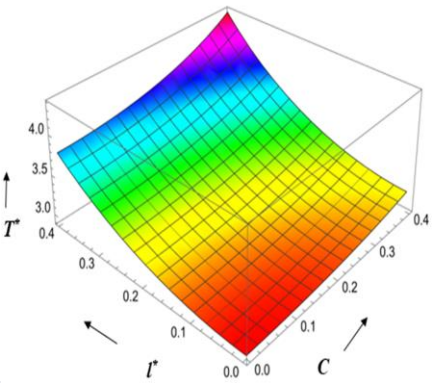

Fig. 40. T^* vs. C (transverse roughness) and l^*.

These findings provide meaningful design implications. For lubrication systems operating under high stress or involving non-Newtonian or microstructured lubricants, fine-tuning both surface texture and couple stress properties can lead to marked performance enhancements. In longitudinal roughness patterns, minimising surface roughness is beneficial to reduce friction and allow the microstructural fluid to respond uniformly. Meanwhile, in transverse orientations, increased roughness, when properly engineered, offers mechanical interlocking with the fluid's internal structure, increasing pressure, load support and operational life. Across all studied configurations, variations in P^*, W^* and T^* were found to be strongly linked to the fluid's microstructural resilience and its interaction with the topography of the bounding surfaces. Smoother surfaces in the direction of motion reduce energy losses, while controlled roughness in the transverse direction enhances entrapment and stability. These interactions are more profound in couple stress fluids compared to classical Newtonian lubricants, as they exhibit additional degrees of freedom due to intrinsic angular momentum and size-dependent effects. This multidimensional investigation advances existing literature by moving beyond isolated parametric studies. Previous works have typically employed 2D analyses or focused solely on either surface geometry or fluid rheology. In contrast, this study utilises 3D surface plots and parametric combinations to deliver a more comprehensive, visually intuitive, and practically applicable understanding of lubrication dynamics. Plots summarise optimal combinations, enabling quick reference for design engineers. Overall, achieving optimal performance in squeeze film systems requires a strategic combination of key design and operating parameters. Specifically, reducing longitudinal roughness and porosity enhances pressure buildup and fluid film stability, while increasing viscosity variation, couple stress effects and Hartmann number improves the fluid's resistance to deformation and external magnetic influences. Additionally, transverse roughness, when carefully optimised, can serve as a functional advantage by enhancing fluid entrapment and load support. Together, these combined effects contribute to improved pressure distribution, greater load-carrying capacity, and extended squeeze film time, making the lubri-

cation system more efficient and durable under a wide range of engineering applications.

The present investigation demonstrates strong alignment with the analytical results of Lin et al. [31], particularly when the effects of magnetohydrodynamics, viscosity variation, and porosity are excluded from the current model. Under such simplified conditions, the numerical outcomes for pressure, load-carrying capacity, and squeeze film time in the current study closely mirror those reported by Lin et al. [31], particularly for a cylinder on a flat surface configuration. This validation, presented in Table 1, confirms the accuracy and consistency of the proposed numerical framework. The excellent agreement further reinforces the model's credibility in simulating complex physical phenomena across various parametric settings.

Table 1. Current analysis numerically compared with Lin et al. [31] using parameter $C = 0.2$, $G = 0.003$, $M_0 = 2$, $\psi = 0.002$, $\delta = 0.1$, $m = 0.1$.

Analysis		Lin et al [31] analysis	Present analysis			
Parameter		C = 0, M_0 = 0, ψ = 0, G = 0	C = 0, M_0 = 0, ψ = 0, G = 0		C = 0.2, G = 0.003, ψ = 0.002, M_0 = 2, δ = 0.1, m = 0.1	
			LR	TR	LR	TR
P*	l* = 0	0.483621	0.483579	0.483579	5.62156	5.62291
	l* = 0.2	0.485617	0.485619	0.485618	5.64031	5.64168
	l* = 0.4	0.491384	0.491385	0.491385	5.67947	5.68086
W*	l* = 0	0.483621	0.483579	0.483579	5.62156	5.62291
	l* = 0.2	0.485617	0.485619	0.485618	5.64031	5.64168
	l* = 0.4	0.491384	0.491385	0.491385	5.67947	5.68086
T*	l* = 0	0.483621	0.483579	0.483579	5.62156	5.62291
	l* = 0.2	0.485617	0.485619	0.485618	5.64031	5.64168
	l* = 0.4	0.491384	0.491385	0.491385	5.67947	5.68086

LR - Longitudinal roughness, TR – Transverse roughness

The relative percentage enhances R_{W^*}, R_{T^*} with respect to W^* and T^*, respectively are:

$$R_{W^*} = \left(\frac{W^*_{magnetic} - W^*_{non-magnetic}}{W^*_{non-magnetic}}\right) \times 100,$$

$$R_{T^*} = \left(\frac{T^*_{magnetic} - T^*_{non-magnetic}}{T^*_{non-magnetic}}\right) \times 100.$$

To evaluate the enhancement in squeeze film performance, Table 2 presents a comparative analysis of the relative percentage increases in W^* and T^*, expressed through dimensionless ratios R_{W^*} and R_{T^*} across various combinations of Hartmann number and viscosity variation, with $\alpha = 0.2$, $C = 0.3$, $h_m{}^* = 0.8$, $\beta = 0.04$, $\psi = 0.001$, $\delta = 0.1$, $m = 0.1$ and $l^* = 0.2$. For instance, at $M_0 = 2$ and $G = 0.004$, the model shows significant improvements of approximately 85.29% in load-carrying capacity and 85.34% in squeeze film time, respectively. These remarkable enhancements underscore the synergistic benefit of combining magnetic field influence with fluid viscosity variation. The results suggest that magnetic stabilisation not only improves fluid confinement but also complements the stabilising effect of non-Newtonian fluid behaviour in high-performance lubrication regimes.

Table 2: Relative percentage of R_{W^*} and R_{T^*}.

M_0	G	R_{W^*}	R_{T^*}
0	0.002	0.024321522	0.024243271
	0.004	0.072964567	0.073140716
	0.006	0.121607611	0.121832709
1	0.002	0.090454811	0.090926625
	0.004	0.273019095	0.273330945
	0.006	0.456134932	0.456286336
2	0.002	0.282115348	0.282318323
	0.004	0.852940023	0.853367247
	0.006	1.432319049	1.433143993

These findings carry profound engineering significance. In automotive and aerospace systems – such as engine liners, thrust bearings and landing gear – where high loads, high speeds and varying environmental conditions prevail, the combined presence of couple stress effects, viscosity gradients and magnetic fields can substantially enhance performance. Improved pressure generation and increased load-bearing capacity reduce mechanical wear, enhance energy efficiency and extend component life. Similarly, in microelectromechanical systems, where surface-to-volume ratios are high and the influence of surface interactions is dominant, the inclusion of MHD and couple stress effects can enhance the reliability of micro-lubrication. Such enhancements support stable and leak-resistant operation even under high-frequency conditions, which is critical in micro-pumps, micro-turbines and other precision components. In the biomedical domain, especially in the design of artificial joints and implantable microfluidic devices, increased squeeze film time plays a vital role in providing improved shock absorption, smoother articulation and enhanced operational lifespan. The influence of surface roughness and porosity becomes particularly relevant here, as material selection and structural permeability are key factors in biocompatible lubrication. Importantly, the observed performance reduction due to increased porosity emphasises the necessity of carefully selecting materials with an optimal balance between permeability and structural strength. For porous bearings and filters, too much porosity can impair pressure generation and reduce the system's overall effectiveness. This highlights the importance of tuning design parameters based on specific application demands – whether the goal is longer operation, higher load support or improved damping. Overall, the insights gained from this study extend beyond theoretical analysis. They provide practical design guidance for optimising lubrication systems across a wide array of applications. By quantitatively illustrating the interplay between surface roughness, porosity, viscosity variation, magnetic fields and microstructural fluid effects, the results offer a comprehensive framework that engineers can apply to design more robust, efficient and application-specific fluid film systems.

5. Conclusions

The current study investigates the performance of squeeze lubrication between a cylinder and a rough, porous flat surface em-

ploying Christensen's stochastic model. Several important observations are:

- The effect of surface roughness for longitudinal surface roughness tends to decrease the dimensionless pressure, load-carrying capacity, and squeeze film time when compared to a smooth surface. In contrast, transverse roughness improves these performance metrics due to enhanced fluid retention.
- The presence of the Hartmann number, couple stress and viscosity variation positively influences the system. These factors significantly increase the load-bearing capacity, pressure and squeeze film time, highlighting their crucial roles in boosting the overall efficiency of the squeeze film.
- Porosity negatively impacts the system, resulting in a decline in pressure, squeeze film time and load-bearing ability for one-dimensional roughness patterns, owing to fluid seepage through the porous medium. This underscores the importance of minimising porosity in high-performance applications.
- The 3D parametric analysis shows that decreasing the roughness parameter in longitudinal roughness patterns and increasing it in transverse patterns, along with reduced porosity, produces maximum values of P^*, W^* and T^*. Additionally, higher values of G, M_0 and l^* consistently lead to improved P^*, W^* and T^* across both roughness orientations, confirming the benefits of multi-parameter optimisation.
- A comparative numerical analysis with the findings of Lin et al. [31] demonstrates strong agreement, validating the accuracy and reliability of the proposed model and numerical framework.
- Combining magnetic field effects ($M_0 = 2$) with viscosity variation ($G = 0.004$) results in significant enhancement of squeeze film lubrication, achieving relative percentage improvements of approximately 85.29% in load-carrying capacity and 85.34% in squeeze film time under optimal conditions.

Despite the robustness of the current theoretical model, several limitations should be recognised. The model is developed under idealised assumptions, such as isothermal, incompressible flow with no external forces, and the analysis is limited to its reliance on numerical simulations without experimental validation, which may not fully capture real-world dynamics. These findings offer valuable insights for designing efficient lubrication systems. Future research should focus on experimental validation using micro-tribological setups, integration of thermal and dynamic effects, and adoption of higher-order or adaptive numerical schemes to improve accuracy and extend the model's applicability to more complex, real-world lubrication scenarios.

6. Novelty

This study presents a novel investigation into the impact of roughness patterns and the role of porosity on squeeze film performance, uniquely integrating factors like viscosity variation, Hartmann number and couple stress, which are often examined separately in existing research. Specifically, it introduces an in-depth three-dimensional graph analysis, revealing how precise optimisation of roughness and porosity can enhance pressure, load-carrying capability and squeeze film time. This approach provides fresh insights into maximising performance in squeeze film applications. The study introduces these novel factors and demonstrates a strong alignment with Lin et al. [31], showcasing significant advancements over previous models. This integration and comparative analysis underline the practical implications for optimising engineering designs, making a meaningful contribution to the field.

References

[1] Bujurke, N.M., Naduvinamani, N.B., & Basti, D.P. (2007). Effect of surface roughness on the squeeze film lubrication between curved annular plates. *Industrial Lubrication and Tribology*, 59(4), 178−185. doi: 10.1108/00368790710753572

[2] Christensen, H. (1969). Stochastic models for hydrodynamic lubrication of rough surfaces. *Proceedings of the institution of mechanical engineers*, 184(1),1013−1026. doi: 10.1243/PIME_PROC_1969_184_074_02

[3] Daliri, M., & Jalali-Vahid, D. (2015). Combined effects of piezo–viscous coupled stress lubricant and rotational inertia upon squeeze film performance of rough circular discs. *Industrial Lubrication and Tribology*, 67(6): 564–571. doi: 10.1108/ILT-01-2015-0009

[4] Mouda, M., Nabhani, M., & El Khlifi, M. (2021). Surface roughness effects on non-Newtonian MHD non-parallel squeeze film bearing. *Industrial Lubrication and Tribology*, 73(1), 45−51. doi: 10.1108/ILT-02-2020-0071

[5] Dass, T.D., Gunakala, S.R., & Comissiong, D.M. (2022). Combined effect of variable-viscosity and surface roughness on the squeeze film characteristics of infinitely wide rectangular plate with couple stress fluid, velocity-slip and ferrofluid lubricant. *Materials Today: Proceedings*, 56, 1717−1725. doi: 10.1016/j.matpr.2021.10.355

[6] Ullah, I., Rahim, M.T., Khan, H., & Qayyum, M. (2016). Analytical analysis of squeezing flow in porous medium with MHD effect. *University of Bucharest Scientific Bulletin Series A. Applied Mathematics and Physics*, 78(2), 281−292.

[7] Johny, A., Sujatha, E., & Sree, M.G. (2024). Effect of MHD on Porous Circular Stepped Plate Lubricated With Micropolar Fluid. *IAENG International Journal of Applied Mathematics*, 54(9), 1847−1854.

[8] Yadav, P.K., & Srivastava, P. (2024). Impact of porous material and slip condition on the MHD flow of immiscible Couple stress-Newtonian fluids through an inclined channel: Head loss and pressure difference. *Chinese Journal of Physics*, 89, 1198−1221. doi: 10.1016/j.cjph.2024.03.046

[9] Patel, N.C., Patel, J.R., & Deheri, G.M. (2023). An effect of a porous structure, slip velocity and Rosensweig's viscosity on the ferrofluid based squeeze film in porous curved annular plates. *Journal of Nanofluids*, 12(2), 498−505. doi: 10.1166/jon.2023.1906

[10] Khan, M.S., Shah, R.A., & Khan, A. (2019). Effect of variable magnetic field on the flow between two squeezing plates. *The European Physical Journal Plus*, 134(5), 219. doi: 10.1140/epjp/i2019-12595-0

[11] Patel, S.J., & Deheri, G. (2023). Slip effect on Shliomis model based magnetic fluid lubrication of a squeeze film in circular cylinder near a plane. *Acta Technica Corviniensis – Bulletin of Engineering*, 16(4).

[12] Lin, J.R., Chu, L.M., Hung, C.R., & Wang, P.Y. (2013). Derivation of two-dimensional couple-stress hydromagnetic squeeze

film Reynolds equation and application to wide parallel rectangular plates. *Meccanica*, 48(1), 253−258. doi: 10.1007/s11012-012-9613-7

[13] Nabhani, M., & El Khlifi, M. (2016). Non-Newtonian inertial magnetohydrodynamic porous squeeze film lubrication between circular discs. *Tribology International*, 94, 373−382. doi: 10.1016/j.triboint.2015.09.047

[14] Ramasamy, P. (2020). Effects of magnetic force and non-Newtonian characteristics on squeeze film bearings. *Asia-Pacific Journal of Chemical Engineering*, 15(5), e2510. doi: 10.1002/apj.2510

[15] Jyothi, V., Hanumagowda, B.N., & Verma, A. (2023). Analysis of pressure load-carrying capacity and squeezing time on magnetohydrodynamic couple stress fluid flow between sphere and flat plate with slip velocity. *International Journal of Modern Physics B*, 38(26), 2450349. doi: 10.1142/S02179792245 03491

[16] Prakash, J., & Tiwari, K. (1985). Effect of surface roughness on the squeeze film between rotating porous annular discs with arbitrary porous wall thickness, *International Journal of Mechanical Sciences*, 27(3), 135–144. doi: 10.1016/0020-7403(85)90054-2

[17] Shah, R.C. (2022). Ferrofluid lubrication of porous-rough circular squeeze film bearings. *The European Physical Journal Plus*, 137(2), 1−16. doi: 10.1140/epjp/s13360-022-02344-z

[18] Thakkar, P.L., & Patel, H.C. (2020). Effect of surface roughness on characteristics of magnetic fluid based squeeze film between porous circular plates. *Journal of the Serbian Society for Computational Mechanics*, 14(1), 90−98. doi: 10.24874/jsscm.2020.14.01.08

[19] Vadher, P.A., Deheri, G., & Patel, R.M. (2008). The effect of surface roughness on the performance of hydromagnetic squeeze films between two conducting rough porous elliptical plates. *Turkish Journal of Engineering and Environmental Sciences*, 32(4), 219−227 (https://www.researchgate.net/publication/228653661).

[20] Deheri, G.M., & Patel, J.R. (2011). Magnetic fluid based squeeze film in a rough porous parallel plate slider bearing. *Annals of the Faculty of Engineering Hunedoara*, 9(3), 443–448.

[21] Anthony, J., & Elamparithi, S. (2023). Effect of MHD and surface roughness on porous step-slider bearing lubricated with couple-stress fluid. *International Journal of Heat and Technology*, 41(1), 135−142. doi: 10.18280/ijht.410114

[22] Ali, N., Khan, S.U., Sajid, M., & Abbas, Z. (2016). MHD flow and heat transfer of couple stress fluid over an oscillatory stretching sheet with heat source/sink in porous medium. *Alexandria Engineering Journal*, 55(2), 915−924. doi: 10.1016/j.aej.2016.02.018

[23] Naduvinamani, N.B., & Siddangouda, A. (2007). Combined effects of surface roughness and couple stresses on squeeze film lubrication between porous circular stepped plates. *Proceedings of the Institution of Mechanical Engineers, Part J: Journal of Engineering Tribology*, 221(4), 525−534. doi: 10.1243/13506501JET204

[24] Vashi, Y., Patel, R.M., & Deheri, G.M. (2018). Ferrofluid Based Squeeze Film Lubrication between Rough Stepped Plates with Couple Stress Effect. *Journal of Applied Fluid Mechanics*, 11(3), 597−612. doi: 10.29252/jafm.11.03.27854

[25] Prakash, J., & Gururajan, K. (1999). Effect of velocity slip in an infinitely long rough porous journal bearing. *Tribology Transactions*, 42(3), 661−667. doi: 10.1080/1040200 9908982267

[26] Rahul, A.K., & Rao, P.S. (2021). Rabinowitsch fluid flow with viscosity variation: Application of porous rough circular stepped plates. *Tribology International*, 154, 106635. doi: 10.1016/j.triboint.2020.106635

[27] Sangeetha, S., & Kesavan, S. (2018). Pressure distribution with surface roughness for effect between porous infinitely long rectangular plates with MHD couple stress squeeze film lubrication. *IOP Conference Series: Journal of Physics: Conference Series*. 1000, 012006. doi: 10.1088/1742-6596/1000/1/012006

[28] Masood, F.A., & Elamparithi, S. (2023). Effects of Surface Roughness and MHD on Squeeze Film Characteristics for Various Finite Porous Plate Geometries with Couple-Stress Fluid. *International Journal of Heat and Technology*, 41(3), 730−736. doi: 10.18280/ijht.410328

[29] Sangeetha, S., Govindarajan, A., & Sujatha, E. (2020). Effect of roughness on porous triangular plates with MHD and viscosity variation. *AIP Publishing AIP Conference Proceedings*, 2277, 030019. doi: 10.1063/5.0025774

[30] Sekar, S., Nathan, S.L., & Saravanathan, L.P. (2022). Velocity Slip with Viscosity Variation for Rough Porous Circular Stepped Plates Using Couple Stress Fluid. *Mathematical Modelling of Engineering Problems*, 9(6), 1631−1638. doi: 10.18280/mmep.090624

[31] Lin, J.R., Liao, W.H., & Hung, C.R. (2004). The effects of couple stresses in the squeeze film characteristics between a cylinder and a plane surface. *Journal of Marine Science and Technology*, 12(2), 7. doi: 10.51400/2709-6998.2228

[32] Kumar, S., & Sachidananda, S. V. (1979). Effects of viscosity variation and surface roughness in short journal bearings. *Wear*, 52(2), 341–346. doi: 10.1016/0043-1648(79)90071-1.

[33] Rajashekar, M., & Kashinath, B. (2012). Effect of surface roughness on MHD couple stress squeeze-film characteristics between a sphere and a porous plane surface. *Advances in Tribology*, 2012, 935690. doi: 10.1155/2012/935690

[34] Baksh, S.A., & Naganagowda, H.B. (2022). Study of surface roughness with MHD and couple stress fluid on porous curved annular plates. *Acta Polytechnica*, 62(6), 574−588. doi: 10.14311/AP. 2022.62.0574

[35] Barus, C. (1891). Note on the Dependence of Viscosity on Pressure and Temperature, *Proceedings of the American Academy of Arts and Sciences*, 27, 13−18. doi:10.2307/20020462

[36] Barus, C. (1893). Isothermals, Isopiestics and Isometrics relative to Viscosity. *American Journal of Science*, S3−45(266), 87−96. doi: 10.2475/ajs.s3-45.266.87